Shielding from Space Radiations

Progress Report

Principal Investigator: Dr. C. Ken Chang
Forooz F. Badavi
and
Dr. Ram K. Tripathi

Department of Biology, Chemistry
and Environmental Sciences

Period: June 1, 1993 through December 1, 1993

CHRISTOPHER NEWPORT UNIVERSITY
NEWPORT NEWS, VIRGINIA 23606-2998

NASA COOPERATIVE AGREEMENT NUMBER NCC-1-178

December 1, 1993

ABSTRACT

This Progress Report covering the period of June 1, 1993 to December 1, 1993 presents the development of an analytical solution to the heavy ion transport equation in terms of a one-layer Green's function formalism. The mathematical developments are recasted into an efficient computer code for space applications. The efficency of this algorithm is accomplished by a nonperturbative technique of extending the Green's function over the solution domain. The code may also be applied to accelerator boundary conditions to allow code validation in laboratory experiments. Results from the isotopic version of the code with 80 isotopes present for a single layer target material, for the case of an Iron beam projectile at 600 MeV/nucleon in water is presented.

INTRODUCTION

Future NASA missions will be limited by exposure to space radiations unless adequate shielding is provided to protect men and equipments from such radiations. Adequate methods required to estimate the damage caused by such radiations behind various shields can be evaluated prior to commitment to such missions.

From the inception of the Langley Research Center heavy ion (HZE) shielding program (refs. 1-3), there has been a continued, close relationship between code development and laboratory experiment (ref. 3). Indeed, the current research goal is to provide computationally efficient high charge and energy ion (HZE) transport codes which can be validated with laboratory experiments and subsquently applied to space engineering design. In practice, two streams of code development have prevailed due to the strong energy dependence of necessary atomic/molecular cross sections and the near singular nature of the laboratory beam boundary conditions (refs. 4-6). The atomic/molecular cross section dependence is adequately dealt with by using the methods of Wilson and Lamkin (ref. 7), allowing efficient numerical procedures to be developed for space radiations (refs. 6,8-10). Although these codes could conceivably be applied to the laboratory validation, methods to control truncation and discretization errors would bear little resemblance to the space radiation codes attempting to be validated. Clearly, a radical reorientation is required to achieve the validation goals of the current NASA space radiation shielding program, and such an approach is the main thrust of this research and is briefly described below.

A useful technique in space radiation shielding is the use of the impulse response Green's function (refs. 11,12), which satisfies the Boltzman equation of the form

$$\left[\vec{\Omega}\cdot\vec{\nabla} - \frac{\partial}{\partial E}\tilde{S}_j(E) + \sigma_j\right] G_{jm}(E, E_o, \vec{\Omega}, \vec{x})$$

$$= \sum_k \int \sigma_{jk}(E, E', \vec{\Omega}, \vec{\Omega}')\, G_{km}(E', E_o, \vec{\Omega}', \vec{x}) d\vec{\Omega}' dE' \quad (1)$$

where G_{jm} reduces to a monoenergetic unidirectional function at the boundary, $\tilde{S}_j(E)$ is the stopping power, σ_j is the total cross section, and σ_{jk} is the inclusive differential cross section. An arbitrary solution to the Boltzman equation within a closed convex region can be written as

$$\phi_j(E, \vec{\Omega}, \vec{x}) = \sum_m \int G_{jm}(E, E', \vec{\Omega} - \vec{\Omega}', \vec{x} - \vec{\Gamma})$$

$$\times\ f_m(E', \vec{\Omega}', \vec{\Gamma}) d\vec{\Omega}' dE' d\vec{\Gamma} \quad (2)$$

where $f_m(E', \vec{\Omega}', \vec{\Gamma})$ is the incident flux at the boundary (ref. 11). Since transport problem is formulated in terms of a single Green's function algorithm, the validation of the Green's function in the laboratory meets the objective of having a space validated code. Since there is hope of a Green's function based on an analytical solution of the Boltzmann equation (ref. 13), the resulting evaluation of the shield properties should be computationally efficient.

The first step in this process is to develop an equivalent Green's function algorithm in one dimension to match the current capability in space radiation transport calculation (refs. 6,14). The algorithm is based on the closed form solution to the one dimensional equation

$$\left(\frac{\partial}{\partial x} - \frac{\partial}{\partial E}\tilde{S}_j(E) + \sigma_j\right) G_{jm}(E, E_o, x)$$

$$= \sum_k \int \sigma_{jk}(E, E') G_{km}(E', E_o, x) dE' \qquad (3)$$

for a monoenergetic beam at the boundary. The probality of validation for ^{20}Ne beams of this algorithm (with multiple scattering corrections) has already shown good correlation (refs. 5,15), but improvements in the nuclear data base are required for achieving higher correlations with experiment. If considerations are restricted to multiple charged ions then the right hand side of equation (3) can be further reduced to

$$\left[\frac{\partial}{\partial x} - \frac{\partial}{\partial E}\tilde{S}_j(E) + \sigma_j\right] G_{jm}(E, E_o, x)$$

$$= \sum_k \sigma_{jk} G_{km}(E, E_o, x) \qquad (4)$$

for which a solution is presented below.

APPROXIMATE GREENS'S FUNCTION

Equation (4) can be simplified by transforming the energy into the the residual range as

$$r_j = \int_0^E dE'/\tilde{S}_j(E') \qquad (5)$$

and defining new field variables as

$$\psi_j(x, r_j) = \tilde{S}_j(E)\phi_j(x, E) \qquad (6)$$

$$\mathcal{G}_{jm}(x, r_j, r'_m) = \tilde{S}_j(E) G_{jm}(x, E, E') \qquad (7)$$

so that equation (4) becomes

$$\left[\frac{\partial}{\partial x} - \frac{\partial}{\partial r_j} + \sigma_j\right] \mathcal{G}_{jm}(x, r_j, r'_m)$$

$$= \sum_k \frac{\nu_j}{\nu_k} \sigma_{jk} \mathcal{G}_{km}(x, r_j, r'_m) \qquad (8)$$

with boundary condition

$$\mathcal{G}_{jm}(0, r_j, r'_m) = \delta_{jm}\, \delta(r_j - r'_m) \qquad (9)$$

and

$$\psi_j(x, r_j) = \sum_m \int_0^\infty \mathcal{G}_{jm}(x, r_j, r'_m) f_m(r'_m) dr'_m \qquad (10)$$

The solution to equation (8) may be written as

$$\mathcal{G}_{jm}(x, r_j, r'_m) = \sum_i \mathcal{G}^{(i)}_{jm}(x, r_j, r'_m) \qquad (11)$$

where zeroth order term of equation (11) is

$$\mathcal{G}^{(o)}_{jm}(x, r_j, r'_m) = g(j)\, \delta_{jm}\, \delta(x + r_j - r'_m) \qquad (12)$$

and the first order term of equation (11) is

$$\mathcal{G}^{(1)}_{jm}(x, r_j, r'_m) \approx \frac{\nu_j\, \sigma_{jm}\, g_{(j,m)}}{x(\nu_m - \nu_j)} \qquad (13)$$

with the condition that $\mathcal{G}^{(1)}_{jm}(x, r_j, r'_m)$ is zero unless

$$\frac{\nu_j}{\nu_m}(r_j + x) \le r'_m \le \frac{\nu_i}{\nu_m} r_j + x \qquad (14)$$

The second order terms of equation (11) are

$$\mathcal{G}^{(2)}_{jm}(x, r_j, r'_m) \approx \sum_k \frac{\sigma_{jk}\, \sigma_{km}\, g(j, k, m)}{r'_{mu} - r'_{m\ell}} \qquad (15)$$

with the condition that $\mathcal{G}^{(2)}_{jm}(x, r_j, r'_m)$ are nonzero for

$$r'_{m\ell} \le r'_m \le r'_{mu} \qquad (16)$$

where

$$r'_{mu} = \left\{ \begin{array}{ll} \frac{\nu_j}{\nu_m} r_j + x & (\nu_m > \nu_k > \nu_j) \\ \frac{\nu_j r_j + \nu_k x}{\nu_m} & (\nu_k > \nu_m > \nu_j) \\ \frac{\nu_j}{\nu_m} r_j + x & (\nu_m > \nu_j > \nu_k) \end{array} \right\} \qquad (17)$$

and

$$r'_{m\ell} = \left\{ \begin{array}{ll} \frac{\nu_j}{\nu_m}(r_j + x) & (\nu_m > \nu_k > \nu_j) \\ \frac{\nu_j}{\nu_m}(r_j + x) & (\nu_k > \nu_m > \nu_j) \\ \frac{\nu_j r_j + \nu_k\, x}{\nu_m} & (\nu_m > \nu_j > \nu_k) \end{array} \right\} \qquad (18)$$

The third order terms of equation (11) are

$$\mathcal{G}^{(3)}_{jm}(x, r_j, r'_m) \approx \sum_{k,\ell} \frac{\sigma_{jk}\, \sigma_{k\ell}\, \sigma_{\ell m}\, g(j,k,\ell,m)}{r'_{mu} - r'_{m\ell}} \qquad (19)$$

and similarly for higher order terms. In the above the g's of n arguments are given by

$$g(j) = e^{-\sigma_j\, x} \qquad (20)$$

and

$$g(j_1, j_2, \cdots j_n, j_{n+1})$$

$$= \frac{g(j_1, j_2 \cdots j_{n-1}, j_n) - g(j_1, j_2 \cdots, j_{n-1}, j_{n+1})}{\sigma_{j_{n+1}} - \sigma_{j_n}} \qquad (21)$$

In terms of above, the solution to equation (4) may be written as

$$\psi_j(x, r_j) = e^{-\sigma_j x} f_j[R_j^{-1}(r_j + x)]$$

$$+ \sum_{m,i} \mathcal{G}_{jm}^{(i)}(x) \Big\{ F_m[R_m^{-1}(r'_{m\ell})]$$

$$- F_m[R_m^{-1}(r'_{mu})] \Big\} \qquad (22)$$

where

$$\mathcal{G}_{jm}^{(i)}(x) =$$

$$\sum_{j_1, j_2 \cdots j_{n-2}} \frac{\sigma_{jj}, \sigma_{j_1 j_2} \cdots \sigma_{j_{n-2} m}\, g(j, j_1 j_2 \cdots j_{n-2}, m)}{\Delta^{(i)}} \qquad (23)$$

for i=1, the denominator of equation (23) is

$$\Delta^{(1)} = x\,(\frac{\nu_m}{\nu_j} - 1) \qquad (24)$$

and for i>1, the denominator becomes

$$\Delta^{(i)} = \left\{ \begin{array}{ll} x\left(1 - \frac{\nu_j}{\nu_m}\right) & (\nu_m > \nu_k > \nu_j) \\ x\left(\frac{\nu_k}{\nu_m} - \frac{\nu_j}{\nu_m}\right) & (\nu_k > \nu_m > \nu_j) \\ x\left(1 - \frac{\nu_k}{\nu_m}\right) & (\nu_m > \nu_j > \nu_k) \end{array} \right\} \qquad (25)$$

In equation (22), $F_m(E)$ is the integral flux at the boundary, and is defined as

$$F_m(E) = \int_E^\infty f_m(E')dE' \qquad (26)$$

Implementation of equation (22) can now be accomplished independent of the character of the boundary values $f_m(E')$ and will give accurate results for both space and laboratory applications.

DISCUSSION OF RESULTS

Values of collision related fluxes for 3 depths of water target for a mono-energetic beam of Iron projectile with 600 MeV/nucleon are shown in figures 1 through 3 for both the perturbative and nonperturbative Green's function methods for the direct comparison of the two methods. The first three collision terms and the sum of all collision terms of both theories at a depth of 5 cm of water are shown in figure 1.A through 1.H. The differences in the spectral shape is due to the simplification of the attenuation term in the nonperturbative theory. The nonperturbation terms represnt the average spectrum while perturbation theory retains the spectral shape. Figures 2.A through 2.H and 3.A through 3.H are the corresponding comparison of the two methods at depths of 10 and 15 cm of water. Direct comparsions of figures 1 through 3 shows that the sequence of perturbation terms appear to be converging to a result similar to that of nonperturbative result.

The main advantage of nonperturbative methods are in their computational efficencies. The computational time required for the nonperturbative code is about 10 minutes on VAX 4000 compared to 15, 45, 90 minutes for the 1-st, 2-nd and 3-rd collision terms of the perturbation solution.

Figures 4.A through 4.C show the corresponding differential LET spectrum using the method of reference 16. The highest LET peak is due to the primary beam and the ion fragments. The successive peaks below iron are due to lower atomic weight fragments. Such LET spectra can be compared to experimental measurments directly.

REFERENCES

1. J. W. Wilson and C. M. Costner, "Nucleon and Heavy Ion Total and Absorption Cross Section for Selected Nuclei," NASA TN D-8107, December 1975.

2. J. W. Wilson, "Analysis of the Theory of High Energy Ion Transport," NASA TN D-8381, March 1977.

3. J. W. Wilson, "Depth Dose Relations for Heavy Ion Beams," Va. J. of Sci. 28, 136-138 (1977).

4. J. W. Wilson, "Heavy Ion Transport in the Straightahead Approximation," NASA TP-2178, June 1983.

5. J. W. Wilson, L. W. Townsend, H. B. Bidasaria, W. Schimmerling, M. Wong and J. Howard, " Ne Depth Dose Relations in Water, "Health Physics 46, 1101 (1984).

6. J. W. Wilson and F. F. Badavi, "Methods of Galactic Heavy Ion Transport," Radiat. Res. 108, 231 (1986).

7. J. W. Wilson and S. L. Lamkin, "Perturbation Approximation for Charged Particle Transport in One Dimension," Nucl. Sci. and Eng. 57, 292-299 (1975).

8. J. W. Wilson, L. W. Townsend, S. Y. Chun, S. L. Lamkin, B. D. Ganapol, B. S. Hong, W. W. Buck, F. Khan, F. A. Cucinotta and J. E. Nealy, "BRYNTRN: A Baryon Transport Model, " NASA TP-2887, 1989.

9. J. L. Shinn, J. W. Wilson, M. Weyland and F. A. Cucinotta, "Improvements in the computational Accuracy of BRYNTRN (A Baryon Transport Code," NASA TP-3093, 1991.

10. J. L. Shinn and J. W. Wilson, "An Efficient HZETRN (A Galactic Cosmic Ray Transport Code)," NASA TP-3147, 1991.

11. J. W. Wilson and G. S. Khandelwal, "Dose Approximations in Arbitrary Convex Geometry," Nucl. Tech. 23,298 (1974).

12. J. W. Wilson, S. L. Lamkin, B. D. Ganopal, H. Farhat and L. W. Townsend , "A Hierarchy of HZE Transport Approximations," NASA TM-4118, 1989.

13. J. W. Wilson, L. W. Townsend and B. D. Ganopal, "A Closed Form Solution to the HZE Propagation," Radiat. Res. 122, 223 (1990).

14. J. W. Wilson, S. Y. Chun, F. F. Badavi and L. W. townsend, "HZETRN: A Heavy Ion/Nucleon transport Code for Space Radiations," NASA TP-3146, 1991.

15. W. Schimmerling, "Ground Based Measurments of Galactic Cosmic Ray Fragmentation in Shielding," COSPAR, 1990.

16. J. W. Wilson, F. F. Badavi, "A Study of Generation of Linear Energy Transfer Spectra for Space Radiations," NASA TM-4410, 1992.

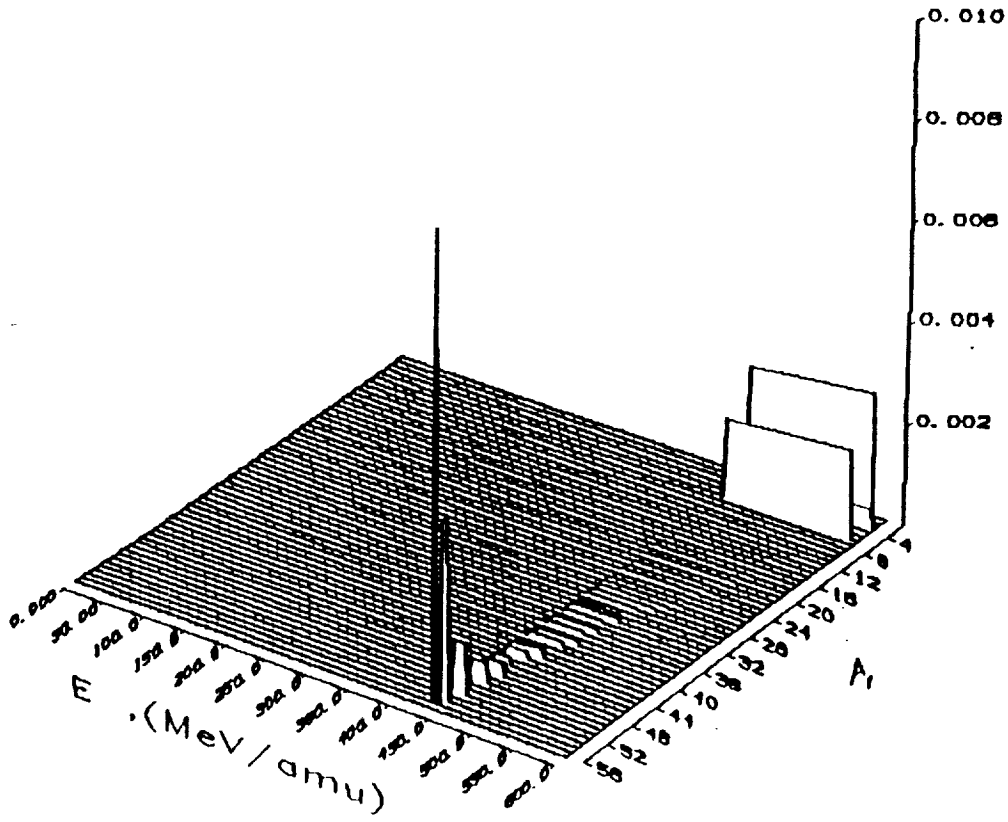

Figure 1.A. 1-st term nonpertubation solution at a depth of 5 cm of water for a 600 MeV/nucleon Iron projectile.

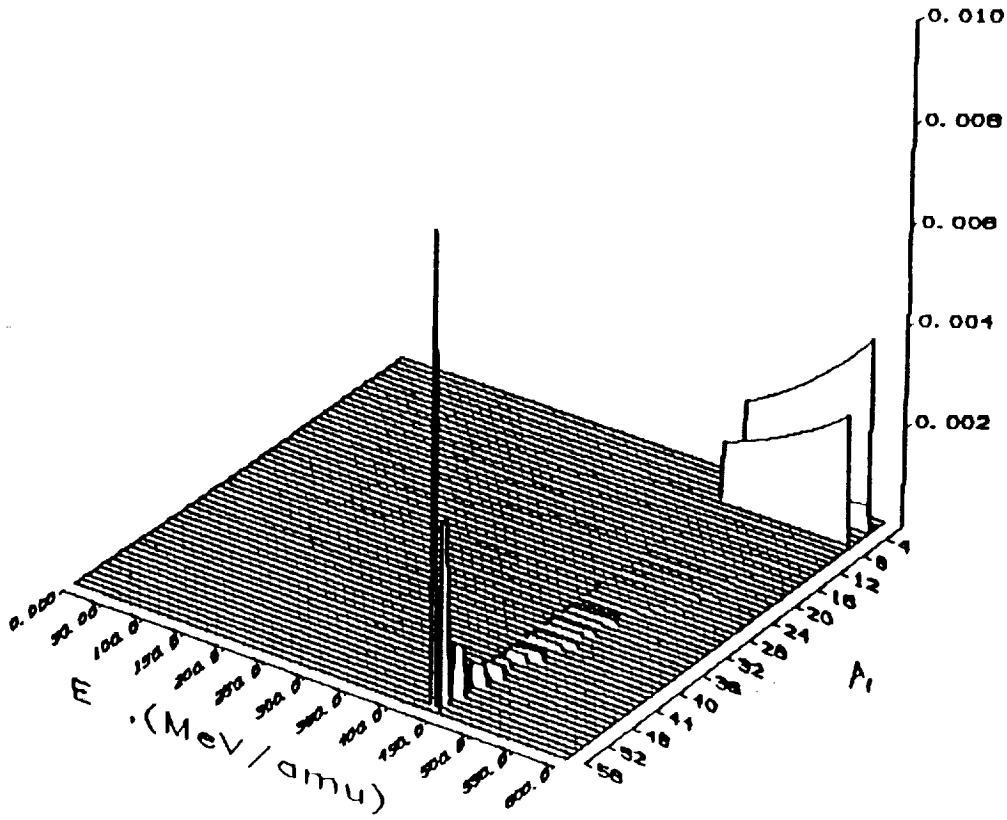

Figure 1.B. 1-st term perturbation solution at a depth of 5 cm of water for a 600 MeV/nucleon Iron projectile.

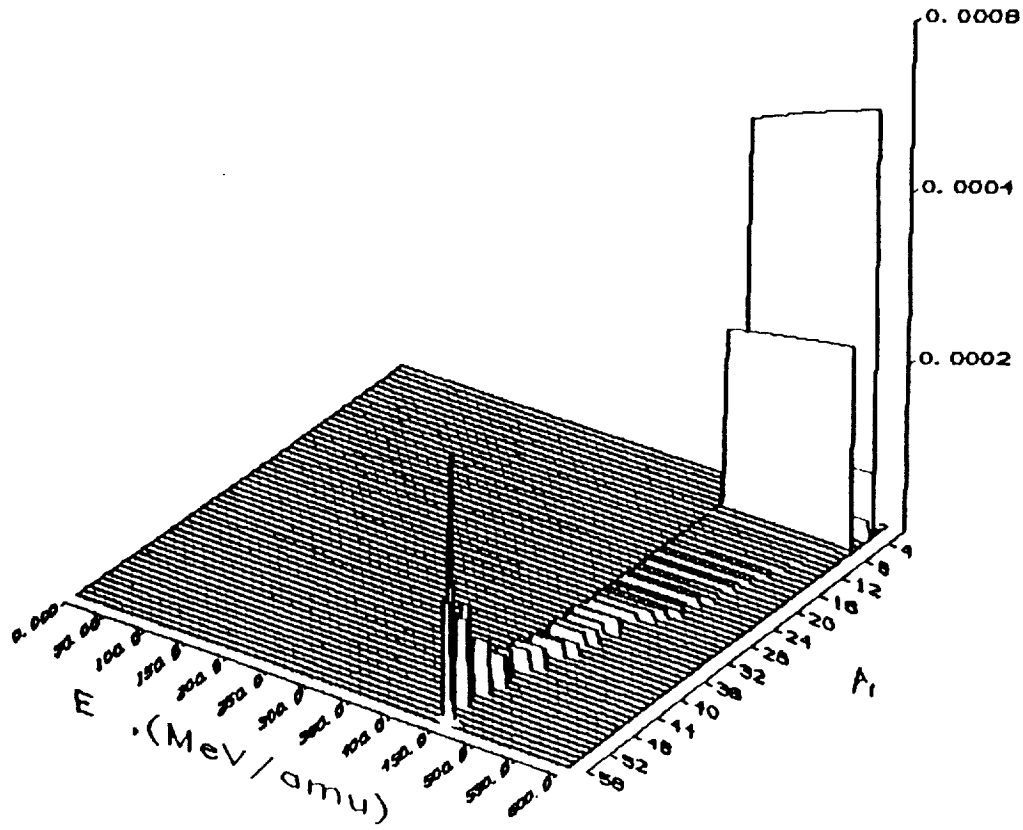

Figure 1.C. 2-nd term nonperturbation solution at a depth of 5 cm of water for a 600 MeV/nucleon Iron projectile.

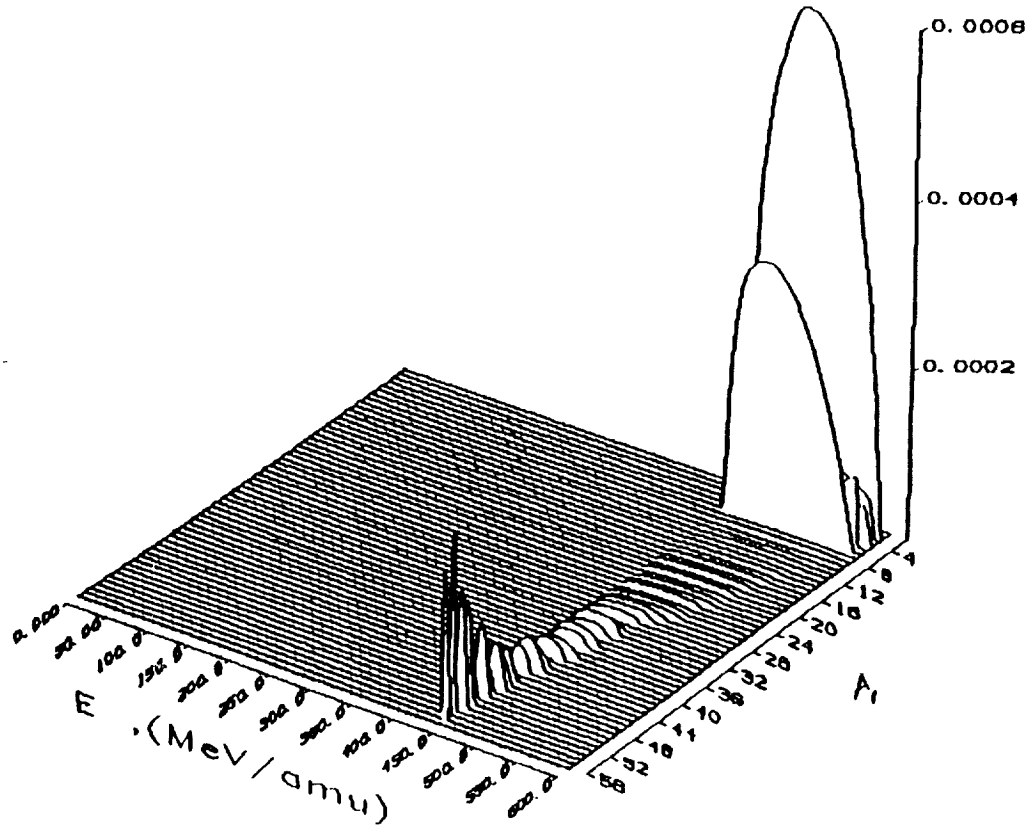

Figure 1.D. 2-nd term perturbation solution at a depth of 5 cm of water for a 600 MeV/nucleon Iron projectile.

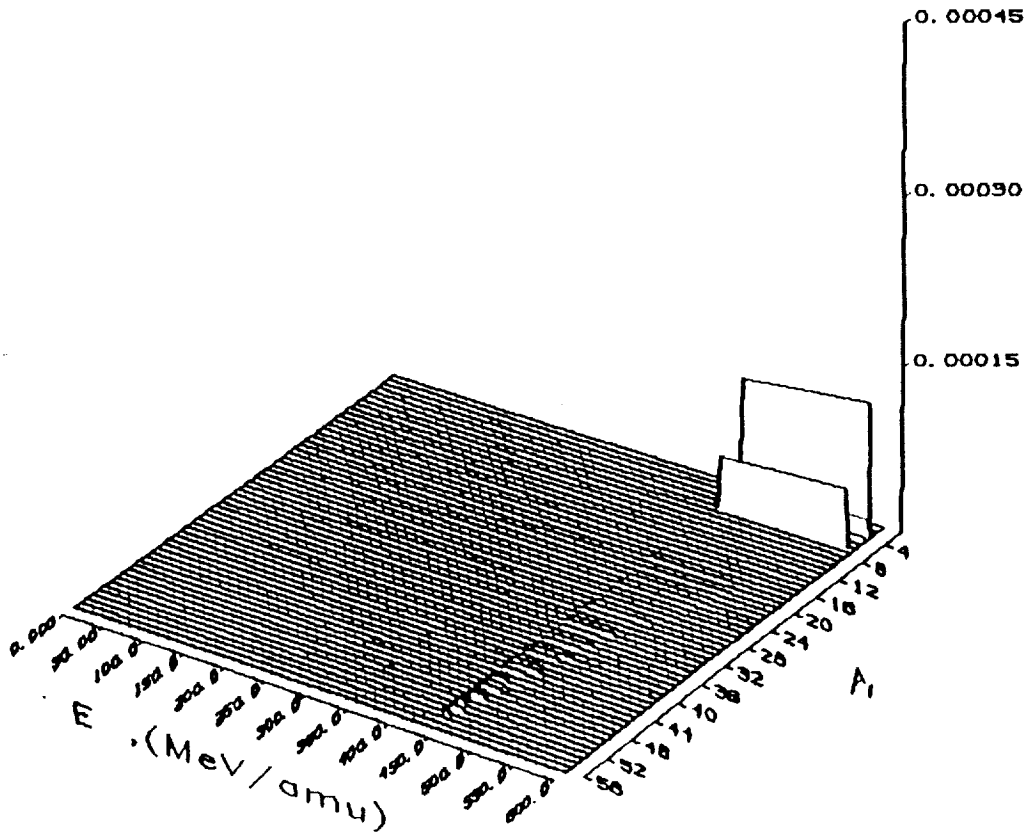

Figure 1.E. 3-rd term nonperturbation solution at a depth of 5 cm of water for a 600 MeV/nucleon Iron projectile.

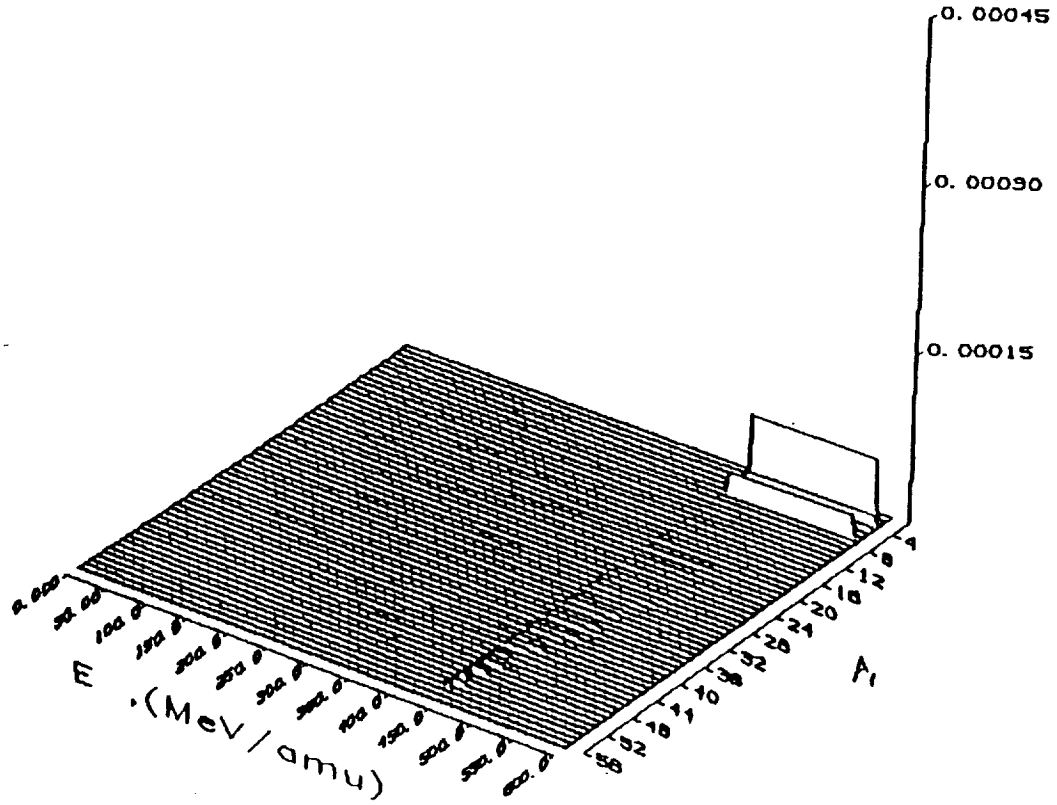

Figure 1.F. 3-rd term perturbation solution at a depth of 5 cm of water for a 600 MeV/nucleon Iron projectile.

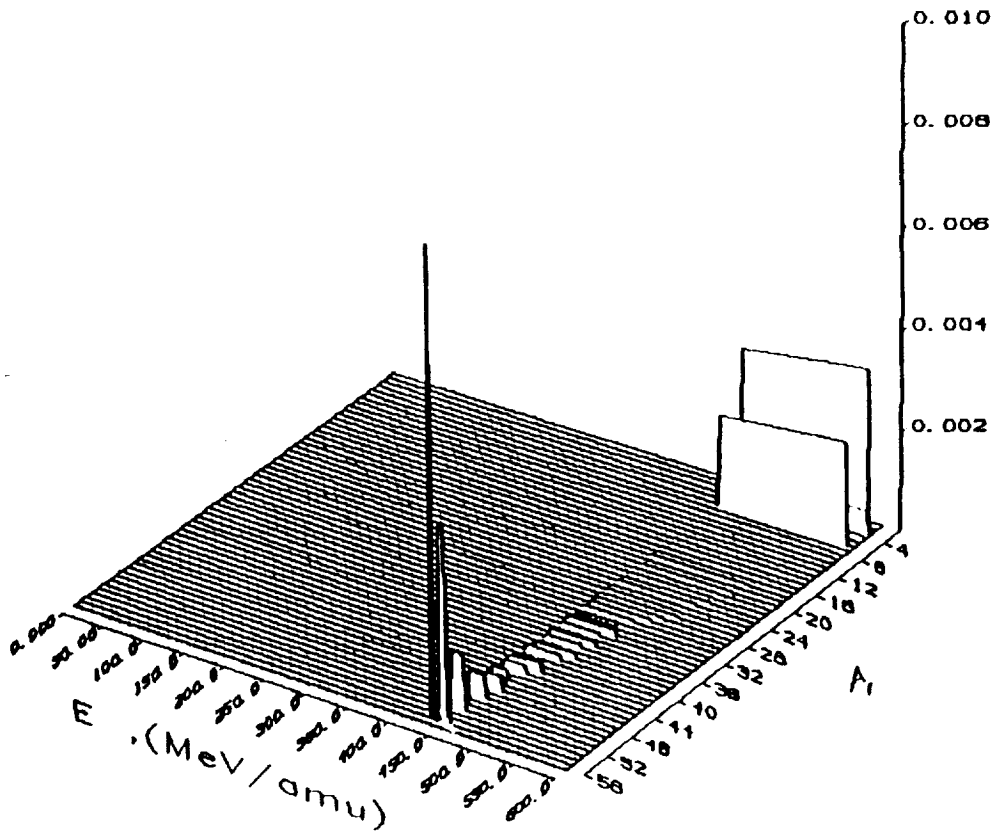

Figure 1.G. All terms nonperturbation solution at a depth of 5 cm of water for a 600 MeV/nucleon Iron projectile.

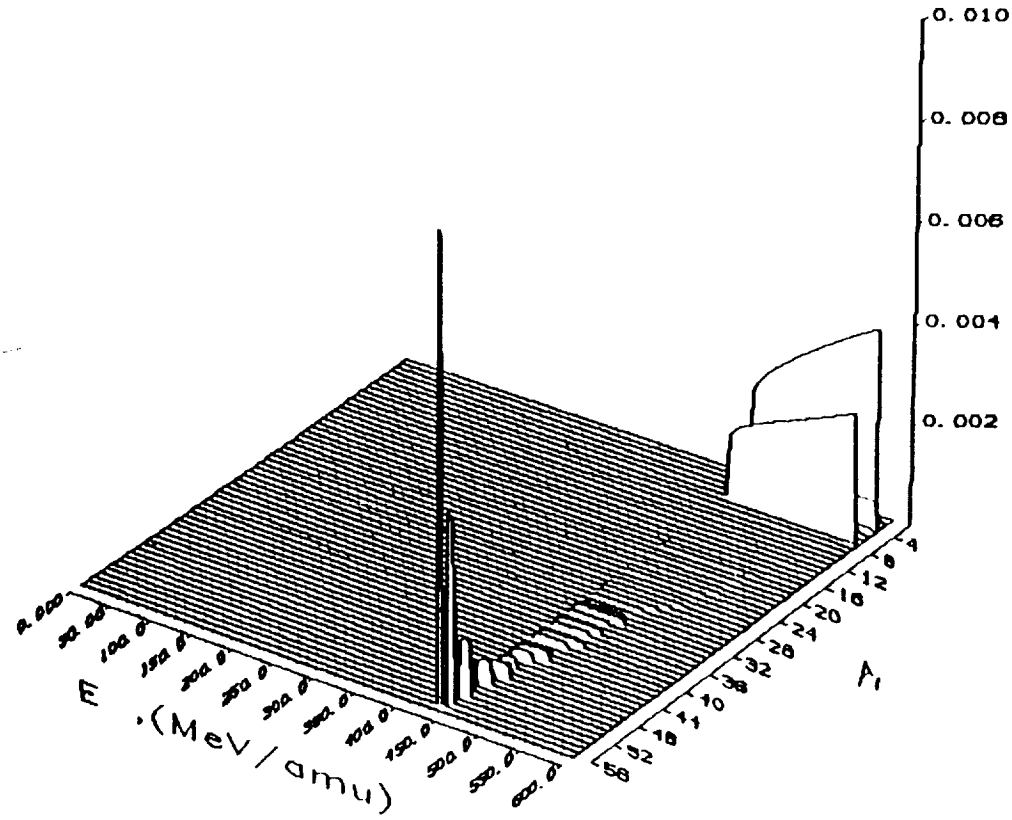

Figure 1.H. All terms perturbation solution at a depth of 5 cm of water for a 600 MeV/nucleon Iron projectile.

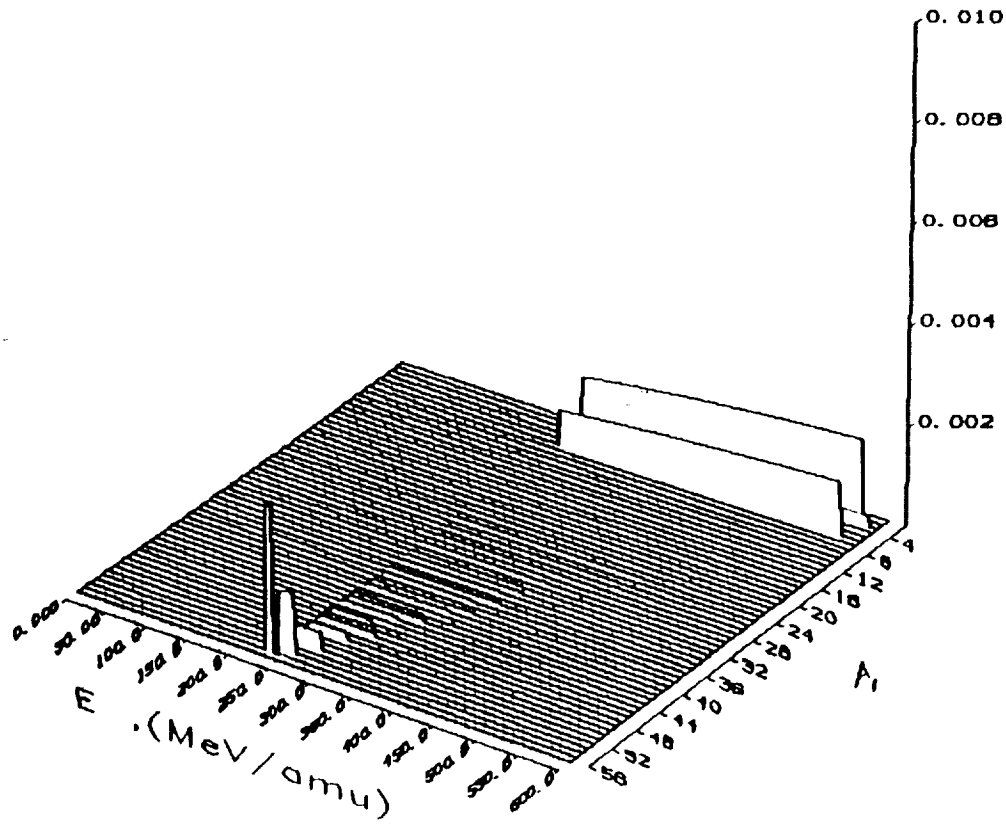

Figure 2.A. 1-st term nonperturbation solution at a depth of 10 cm of water for a 600 MeV/nucleon Iron projectile.

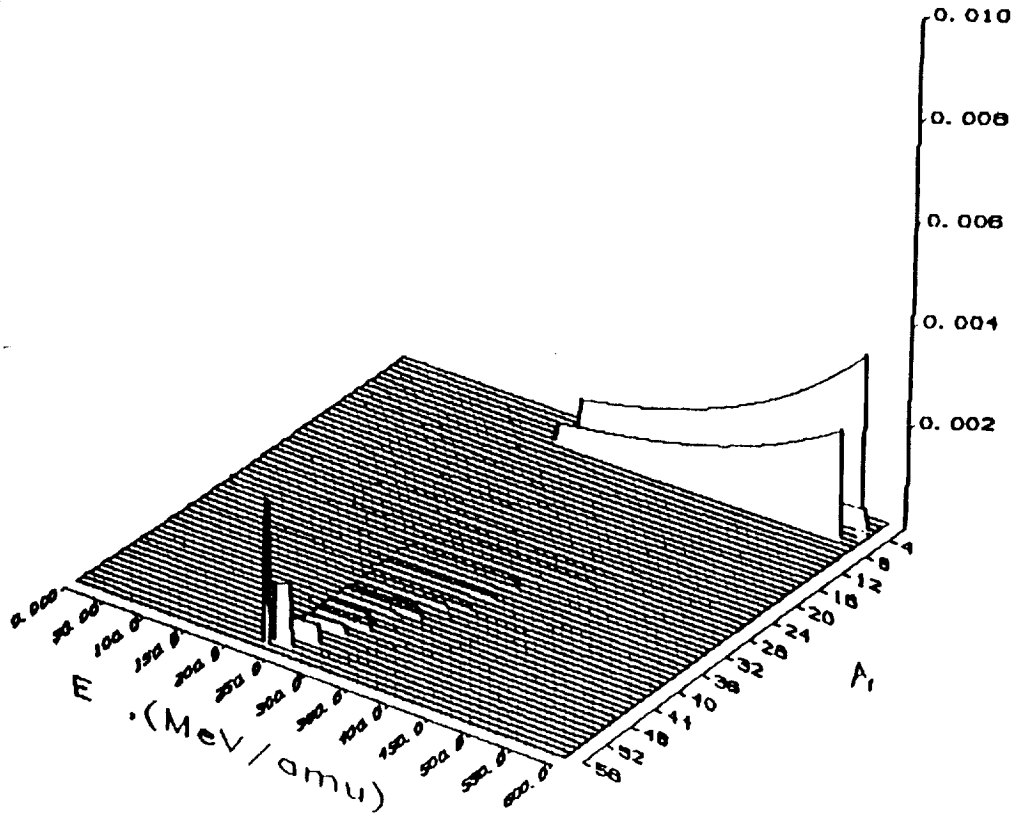

Figure 2.B. 1-st term perturbation solution at a depth of 10 cm of water for a 600 MeV/nucleon Iron projectile.

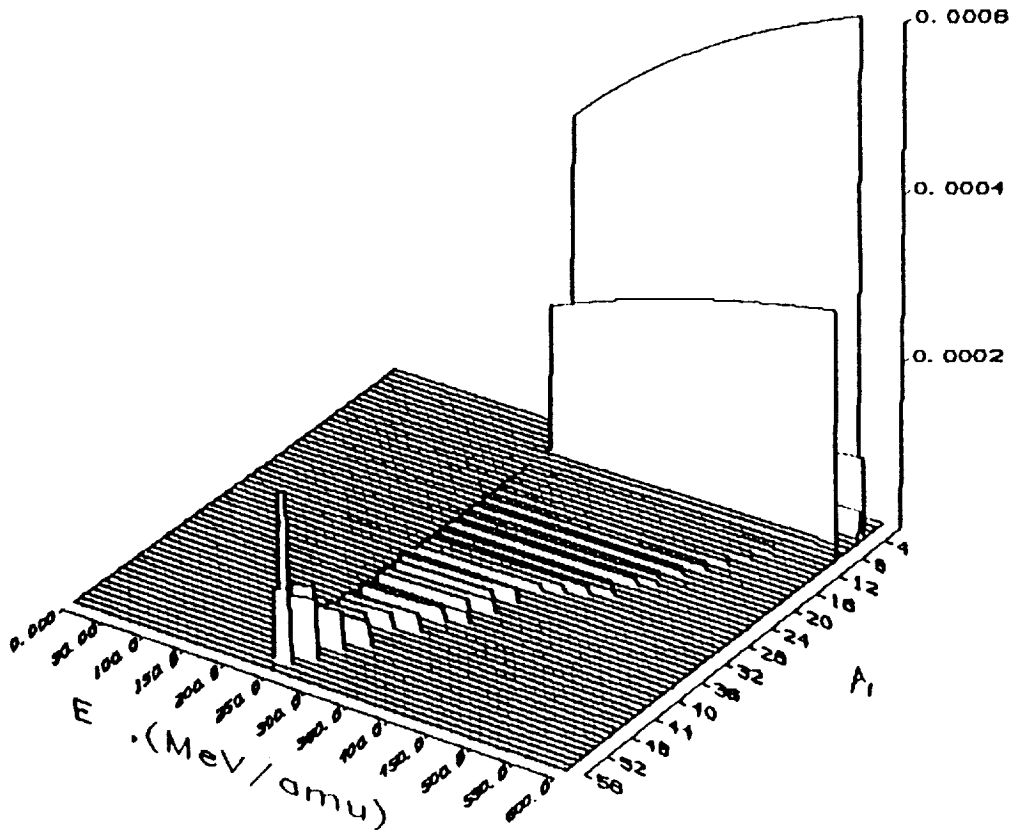

Figure 2.C. 2-nd term nonperturbation solution at a depth of 10 cm of water for a 600 MeV/nucleon Iron projectile.

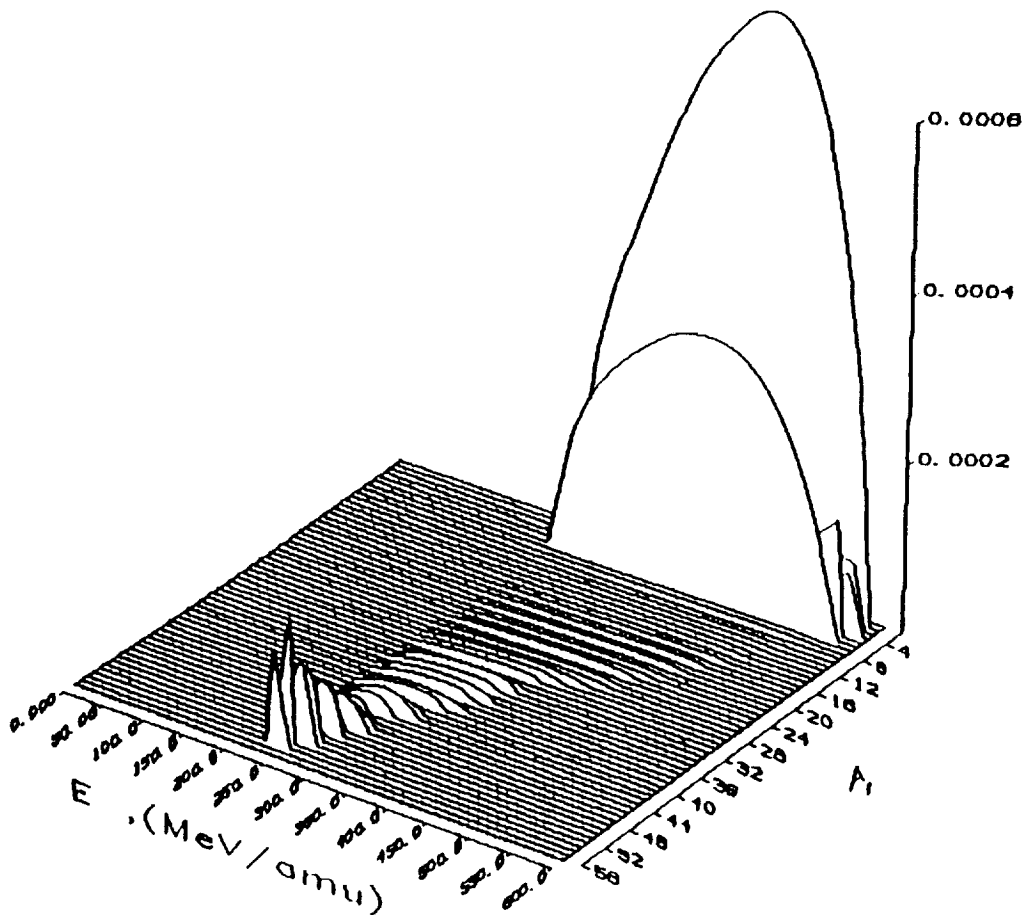

Figure 2.D. 2-nd term perturbation solution at a depth of 10 cm of water for a 600 MeV/nucleon Iron projectile.

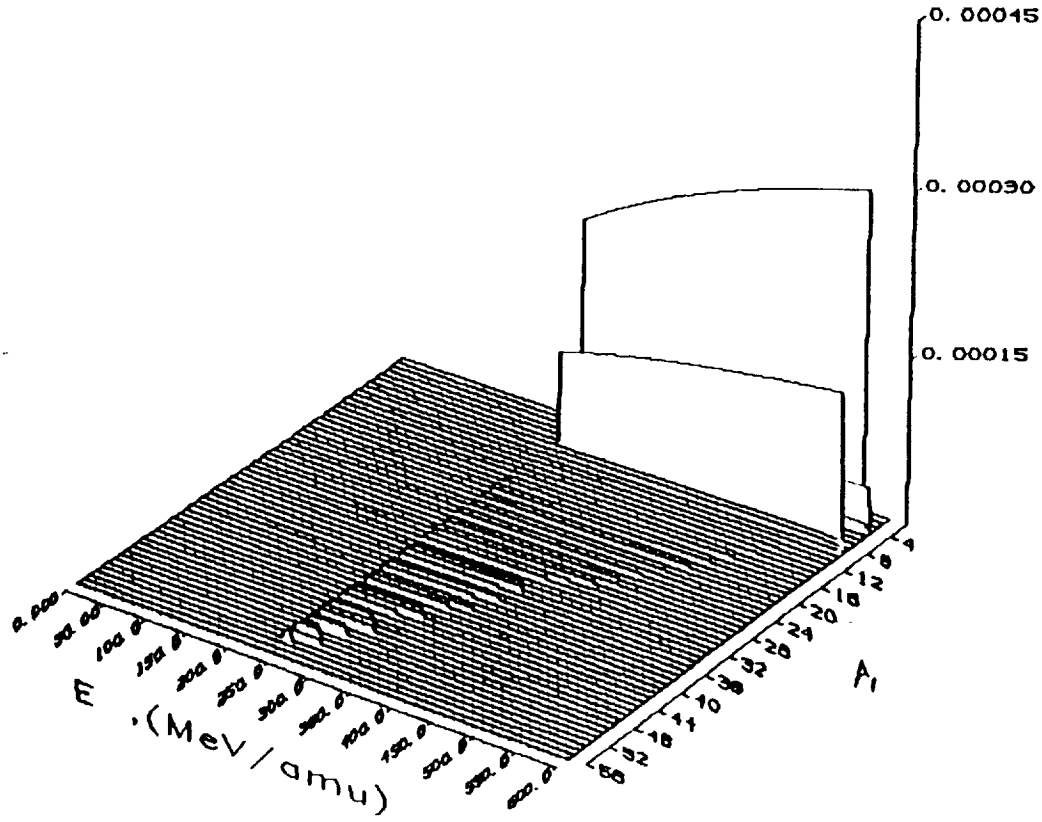

Figure 2.E. 3-rd term perturbation solution at a depth of 10 cm of water for a 600 MeV/nucleon Iron projectile.

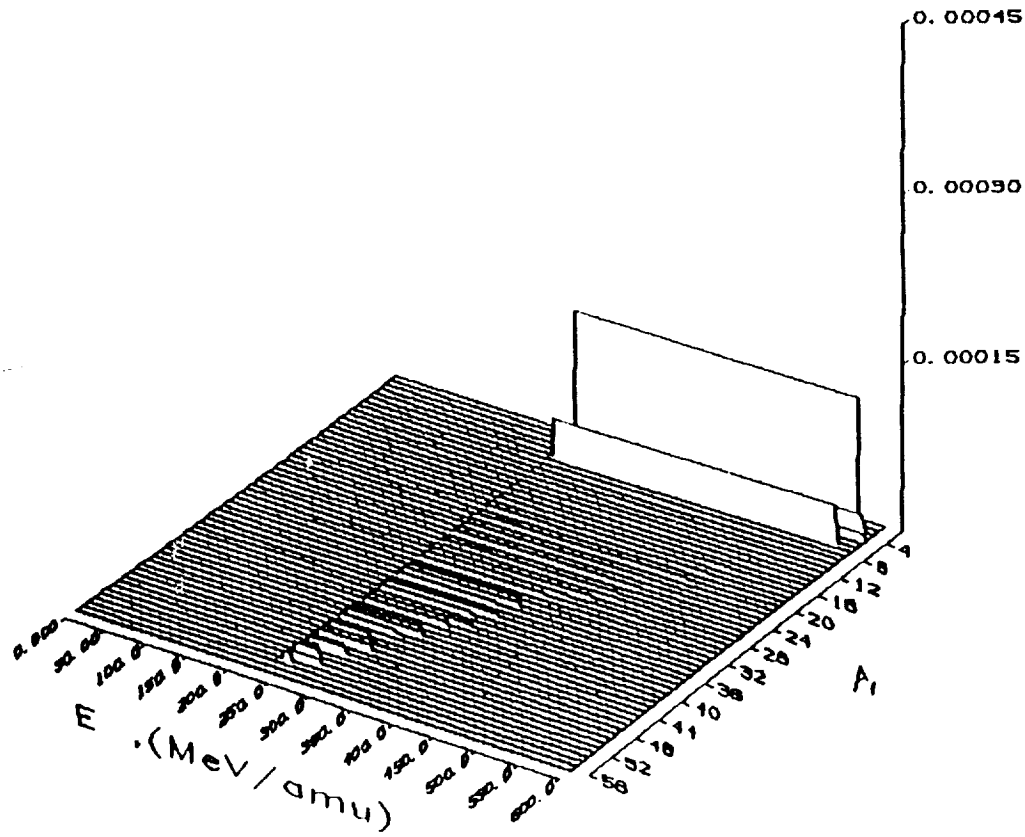

Figure 2.F. 3-rd term perturbation solution at a depth of 10 cm of water for a 600 MeV/nucleon Iron projectile.

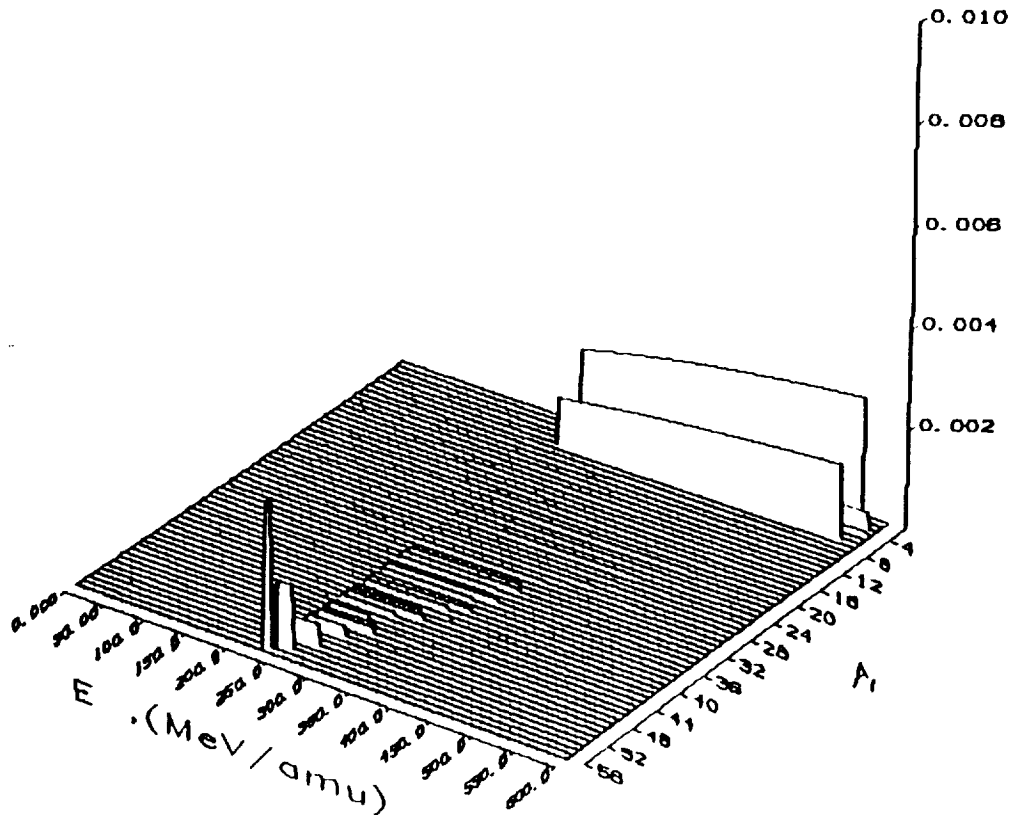

Figure 2.G. All terms nonperturbation solution at a depth of 10 cm of water for a 600 MeV/nucleon Iron projectile.

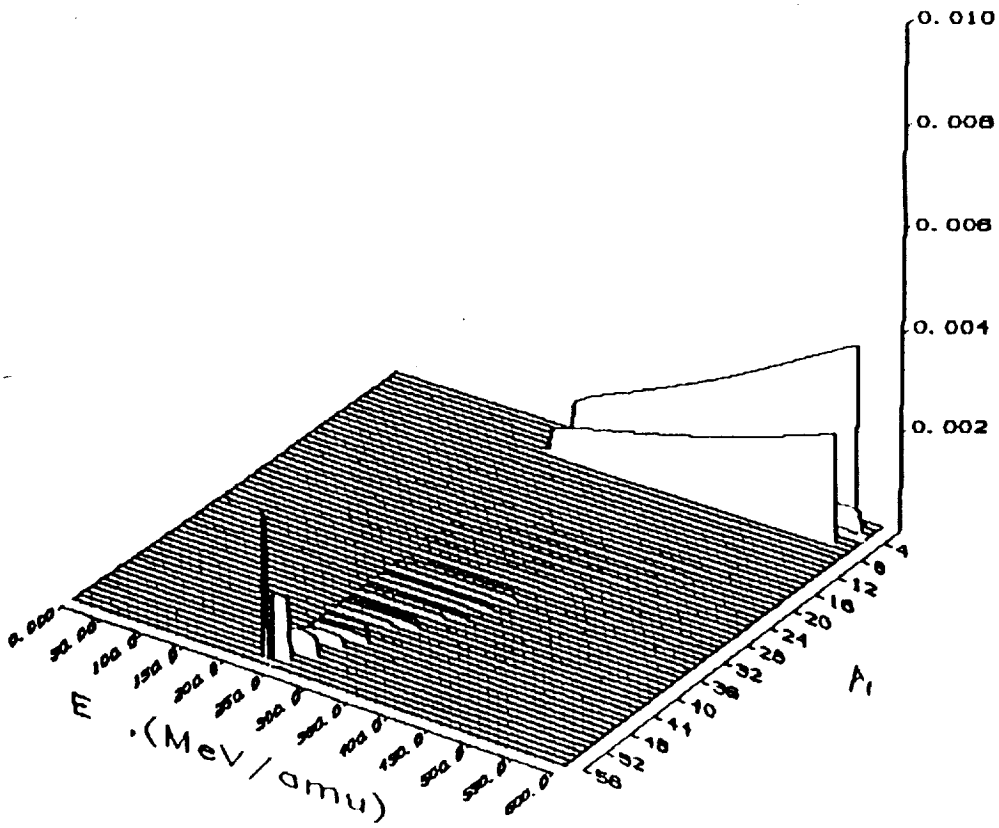

Figure 2.H. All terms perturbation solution at a depth of 10 cm of water for a 600 MeV/nucleon Iron projectile.

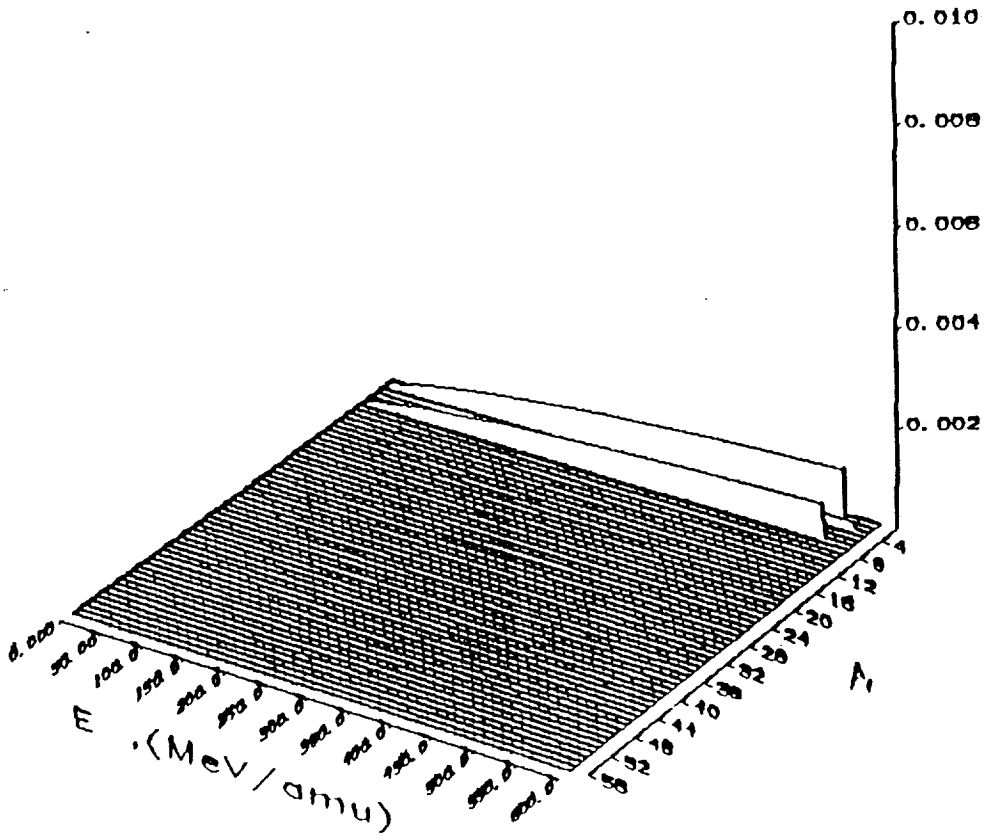

Figure 3.A. 1-st term nonperturbation solution for a depth of 15 cm of water for a 600 MeV/nucleon Iron projectile.

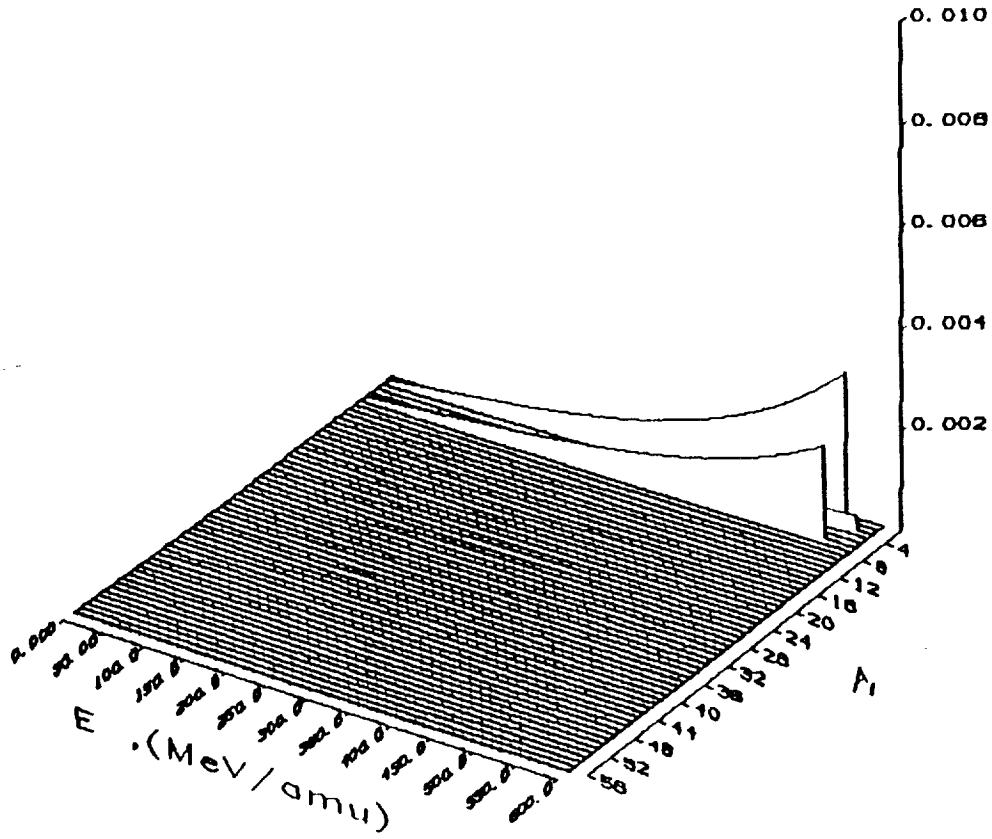

Figure 3.B. 1-st term perturbation solution for a depth of 15 cm of water for a 600 MeV/nucleon Iron projectile.

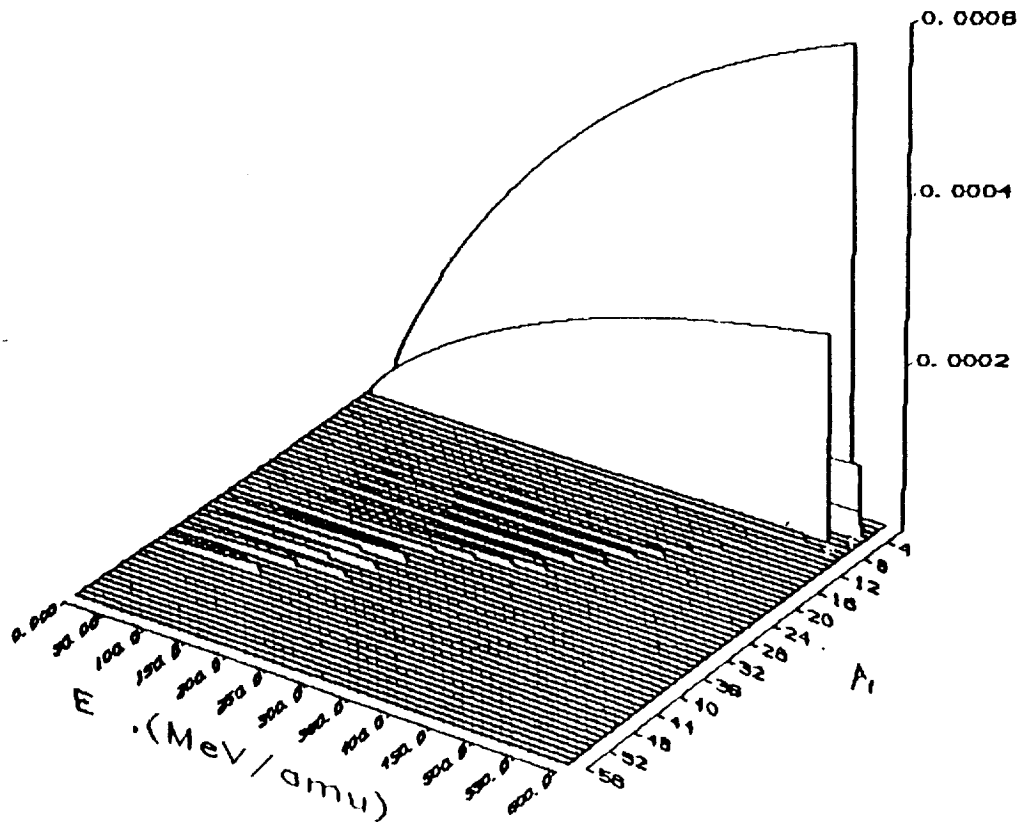

Figure 3.C. 2-nd term nonperturbation solution for a depth of 15 cm of water for a 600 MeV/nucleon Iron projectile.

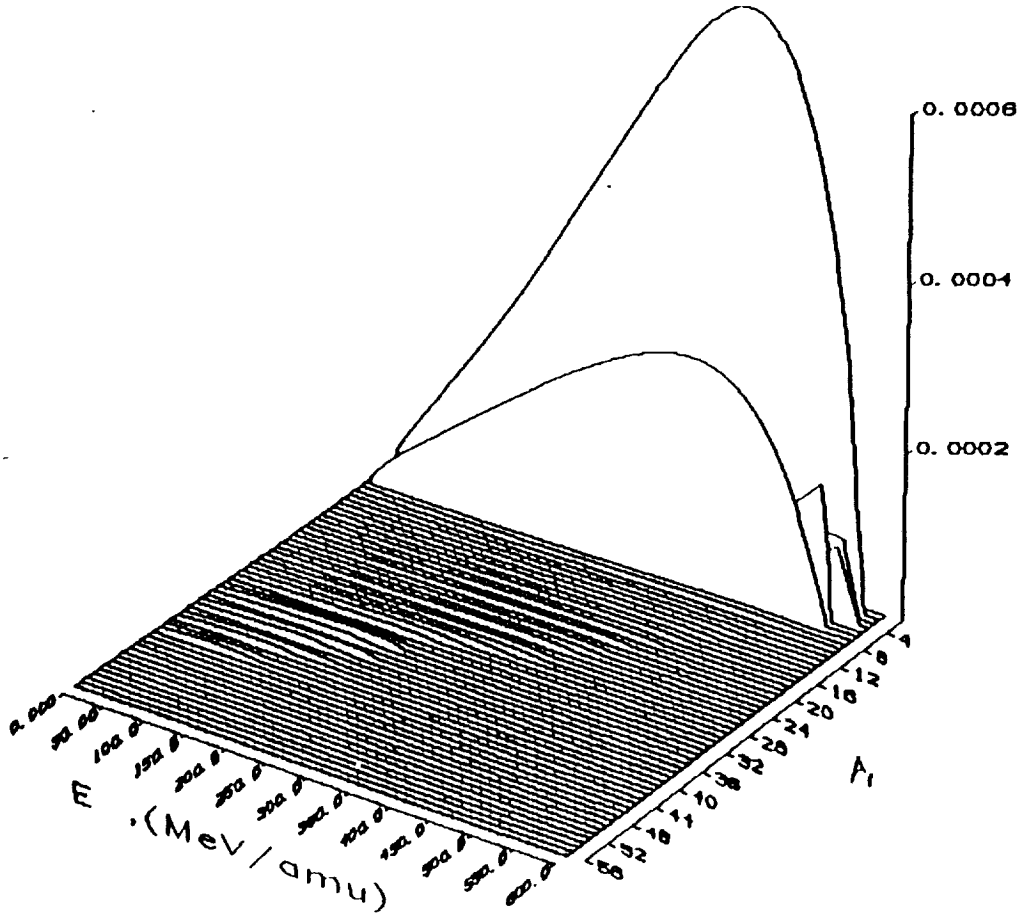

Figure 3.D. 2-nd term perturbation solution for a depth of 15 cm of water for a 600 MeV/nucleon Iron projectile.

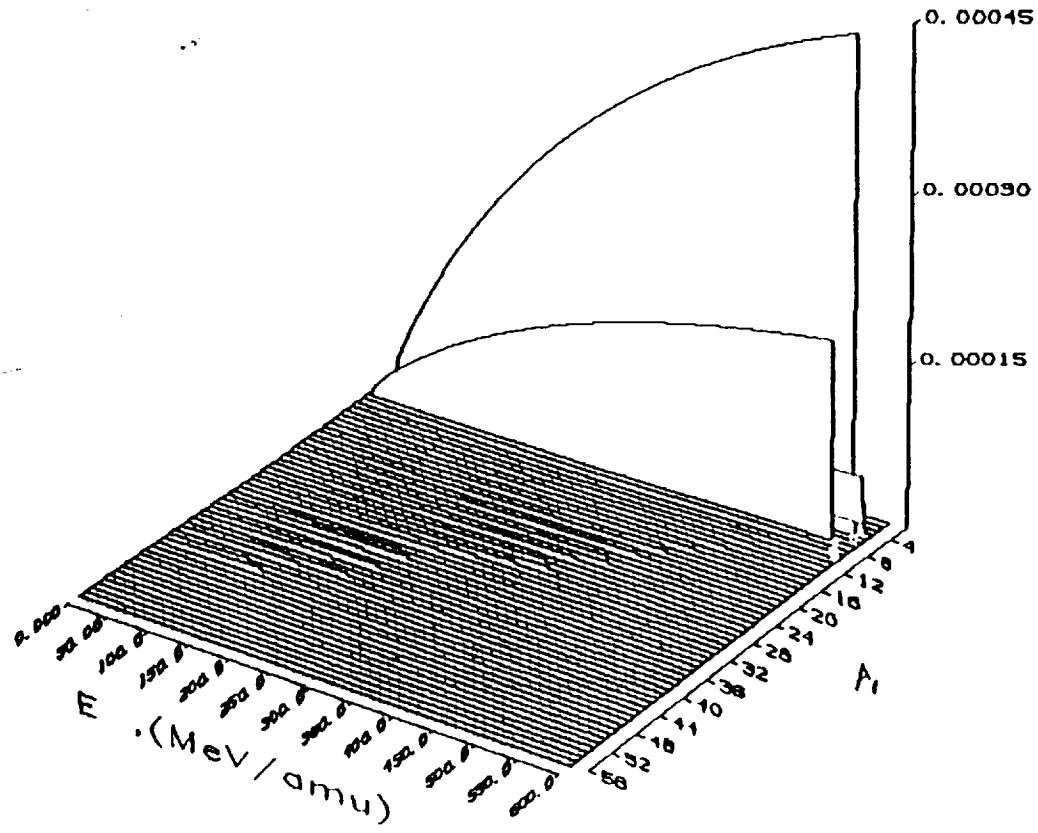

Figure 3.E. 3-rd term nonperturbation solution for a depth of 15 cm of water for a 600 MeV/nucleon Iron projectile.

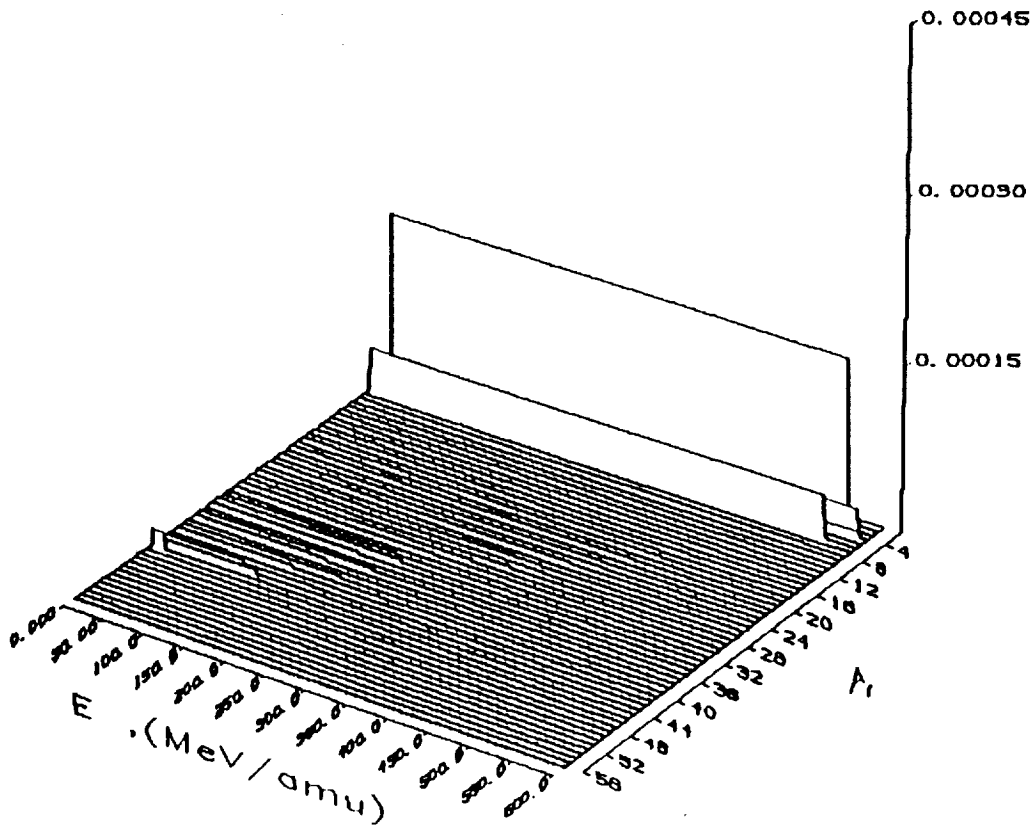

Figure 3.F. 3-rd term perturbation solution for a depth of 15 cm of water for a 600 MeV/nucleon Iron projectile.

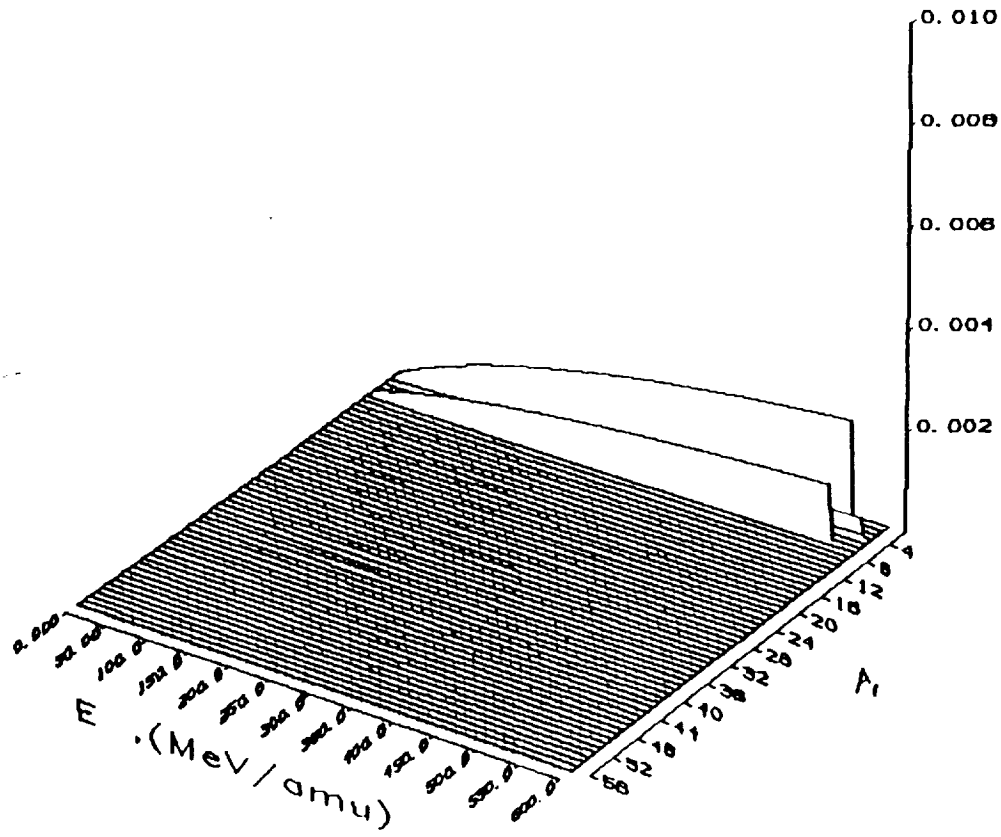

Figure 3.G. All terms nonperturbation solution for a depth of 15 cm of water for a 600 MeV/nucleon Iron projectile.

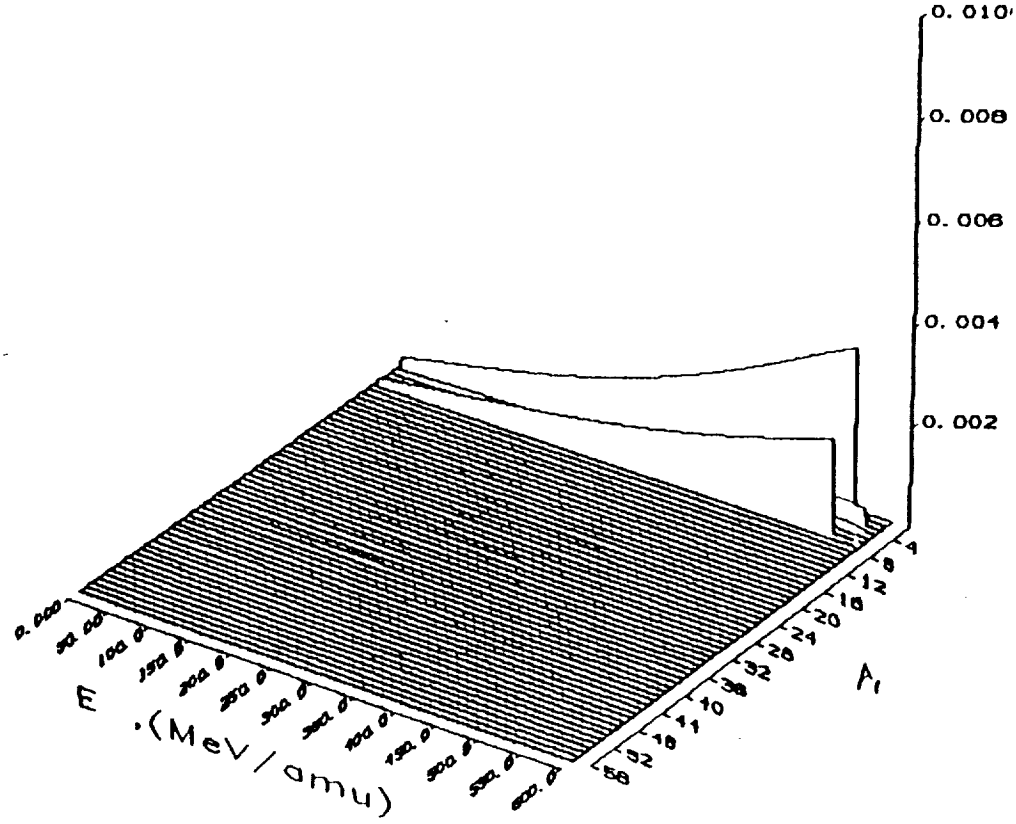

Figure 3.H. All terms perturbation solution for a depth of 15 cm of water for a 600 MeV/nucleon Iron projectile.

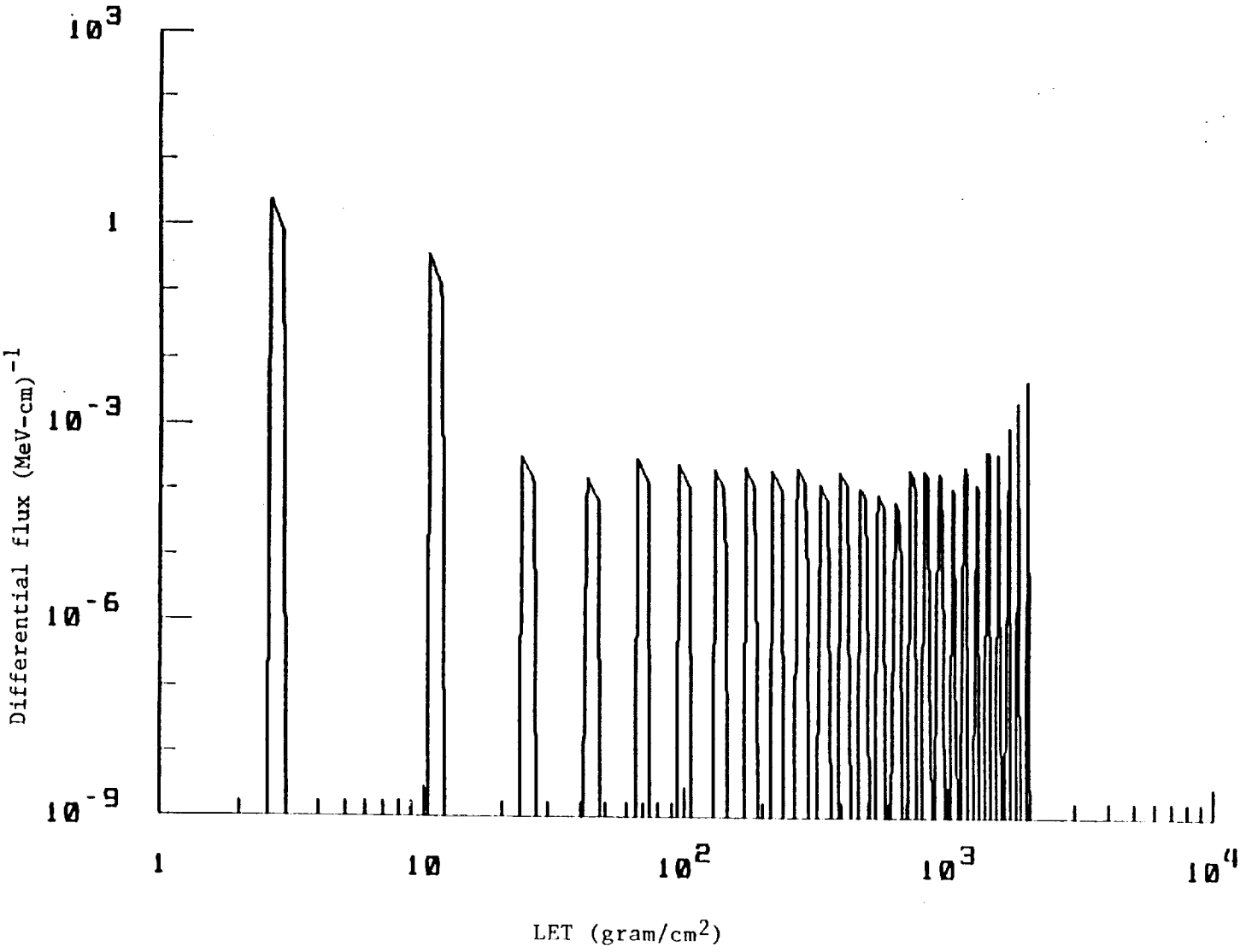

Figure 4.A. Differential LET spectrum for a depth of 5 cm of water for a 600 MeV/nucleon Iron projectile.

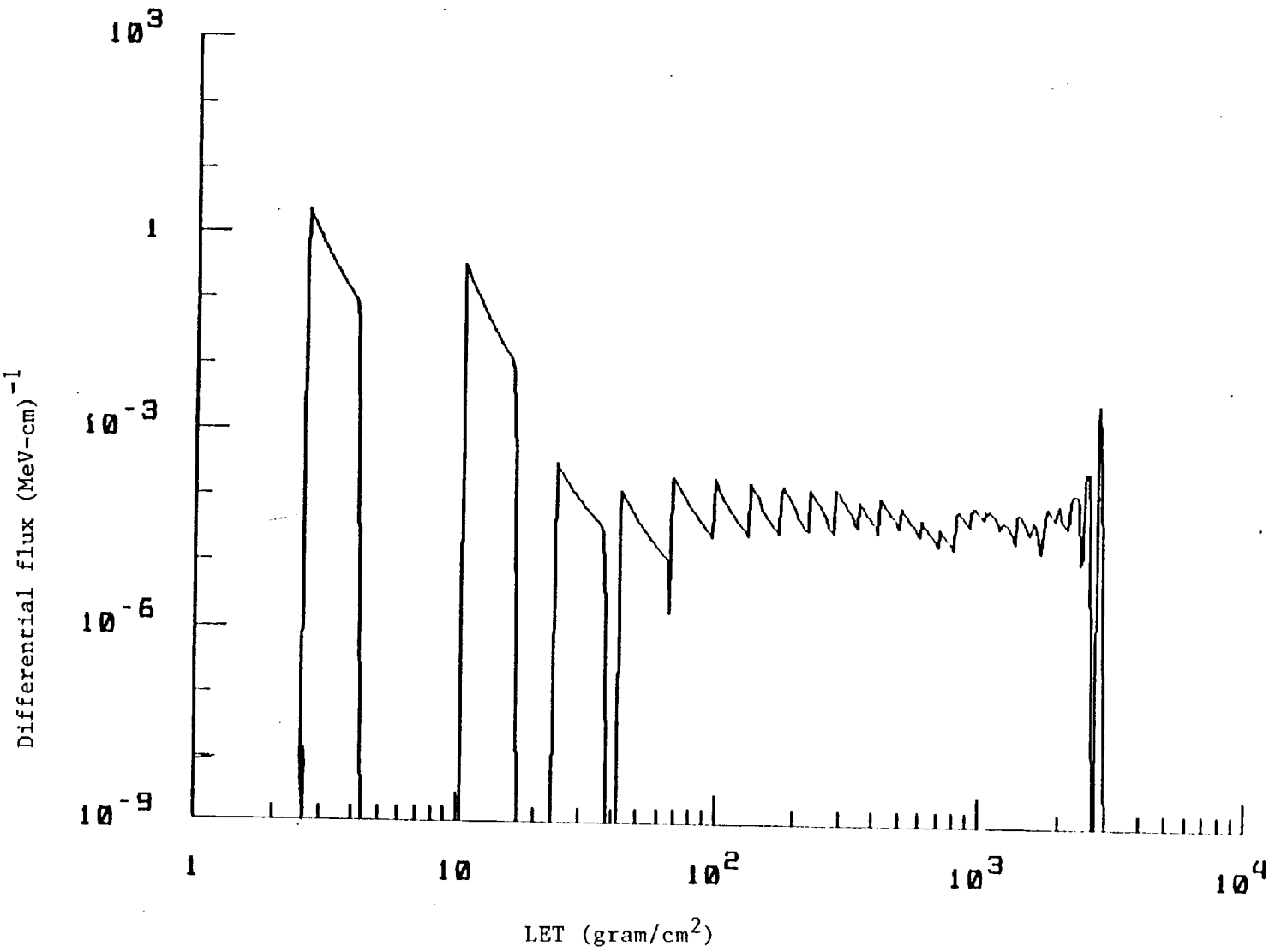

Figure 4.B. Differential LET spectrum for a depth of 10 cm of water for a 600 MeV/nucleon Iron projectile.

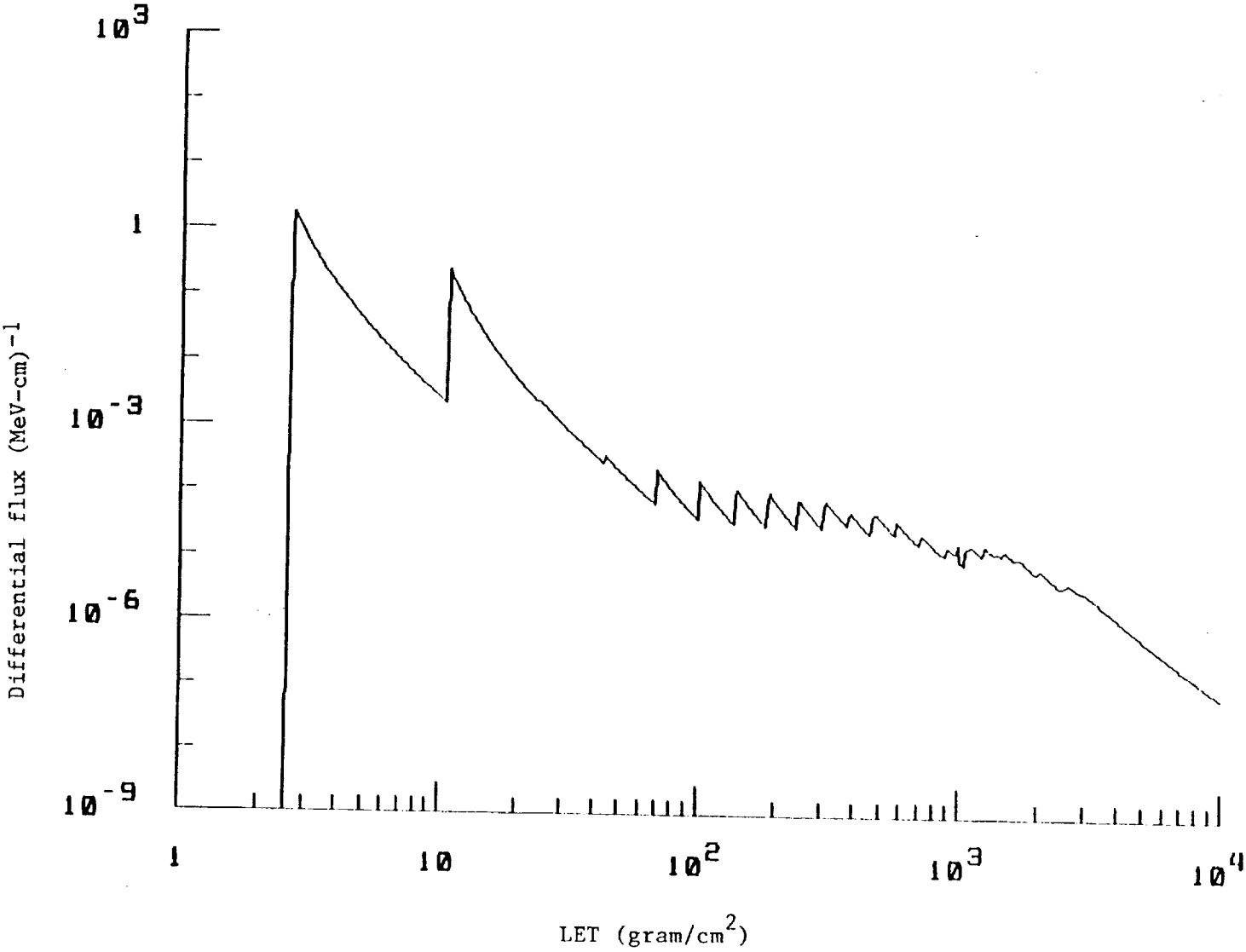

Figure 4.C. Differential LET spectrum for a depth of 15 cm of water for a 600 MeV/nucleon Iron projectile.